

Transient Thermal Bubble Formation on Polysilicon Micro-Resisters

Jr-Hung Tsai

Mechanical Engineering Department,
University of Michigan,
Ann Arbor, MI
e-mail: jhtsai@argon.eecs.berkeley.edu

Liwei Lin

Mechanical Engineering Department,
University of California at Berkeley,
Mechanical Engineering,
1113 Etcheverry Hall,
University of California,
Berkeley, CA 94720-1740

Transient bubble formation experiments are investigated on polysilicon micro-resisters having dimensions of 95 μm in length, 10 μm or 5 μm in width, and 0.5 μm in thickness. Micro resistors act as both resistive heating sources and temperature transducers simultaneously to measure the transient temperature responses beneath the thermal bubbles. The micro bubble nucleation processes can be classified into three groups depending on the levels of the input current. When the input current level is low, no bubble is nucleated. In the middle range of the input current, a single spherical bubble is nucleated with a waiting period up to 2 sec while the wall temperature can drop up to 8°C depending on the magnitude of the input current. After the formation of a thermal bubble, the resistor temperature rises and reaches a steady state eventually. The bubble growth rate is found proportional to the square root of time that is similar to the heat diffusion controlled model as proposed in the macro scale boiling experiments. In the group of high input current, a single bubble is nucleated immediately after the current is applied. A first-order model is proposed to characterize the transient bubble nucleation behavior in the micro-scale and compared with experimental measurements. [DOI: 10.1115/1.1445136]

Keywords: Bubble Growth, Heat Transfer, Microscale, Phase Change, Transient

1 Introduction

Device miniaturization has been the technology driver in both semiconductor and microelectromechanical system (MEMS) research. As a result, heat dissipation has become a major problem in integrated circuit (IC) industry due to the fact that more micro-electronic devices are densely placed in an extremely tiny area. Because boiling heat transfer is the most effective way for heat removal, several research have been proposed to use the phase change phenomenon as the heat dissipation mechanism for semiconductor chips [1,2]. On the other hand, boiling phenomenon has also been applied as the driving mechanism in various MEMS devices, such as thermal bubbles for ink-jet printers [3], bubble powered microactuators [4], and bubble powered pumping effects [5]. The possible applications for micro-bubble powered devices are abundant and the potential of using the phase change process to solve the heat dissipation problem in IC industry is enormous. Therefore, it is important to investigate the fundamental mechanisms of bubble nucleation in the micro-scale.

Among the demonstrated devices using thermal bubbles, they can be classified into two groups according to the devices structures. In the case of open environment, there is ink-jet printer head [3]. In the case of close environment, there are micro-thermal bubble pumps [6,7] and micro-thermal bubble valves [8]. In order to make better bubble-powered micro-devices, it is important to study micro-bubble formation in both open environment and inside microchannels, including the transient bubble formation behavior. Previously, Lin et al. investigated the bubble formation mechanisms on polysilicon micro resistor in open environment [5] and inside microchannels [9]. Yang [10] reported an overview of boiling on microstructures. Although these reports contributed various aspects of bubble formation by using micro resistors, none of them discussed the transient behavior of micro-bubble formation that plays an important role in the design and the operation of micro-bubble-based devices. In macro-scale, the bubble nucleation process has been studied from many aspects, such as ul-

mate boiling temperature limit [11], nucleation from trapped gas [12], bubble growth [13], and the local temperature fluctuation at the heating surface [14]. This paper concentrates on the transient temperature fluctuation during bubble formation and bubble growth on a polysilicon micro-resistor. Both mathematical models and experimental results are established for the characterization of transient bubble formation in the micro-scale.

2 Experiments

A Petri dish containing the testing chip and experimental liquid is placed on the observation chuck of a probe station as shown in Fig. 1. The bulk liquid temperature is measured before and after each experiment by a thermal couple, and is found to be within 1°C of variation. The microscope is connected to a CCD camera to capture images during the transient bubble formation experiments. HP4145 semiconductor parameter analyzer is used as the power source and signal recording system. Polysilicon micro-resisters are fabricated by using the MCNC MUMPs service [15] and they work as resistive heaters. The cross sectional view of the device is shown in Fig. 2(a) with silicon nitride as the insulation material and gold as the metal contact. The typical dimension of the polysilicon resistive heater is 95 μm in length, 5 μm , or 10 μm in width and 0.5 μm in thickness. There are two pairs of electrical contact pads for measuring current and voltage simultaneously to monitor the resistance changes of the polysilicon micro resistor as shown in Fig. 2(b). When a current is applied to the resistive heater, the voltage change at the central portion, 2.5 μm away from both ends of the resistor, is recorded. The temperature coefficient of resistance of polysilicon is characterized as $1.2 \cdot 10^{-3}/\text{K}$ by measuring the resistance changes with respect to environmental temperature changes. The transient temperature response of the resistor is calculated based on this coefficient. It is noted that this coefficient is experimentally characterized and valid when temperature is less than 300°C that is within the temperature range of this work. Second-order effects may need to be considered when the operation temperature is high. A fabricated device is shown in Fig. 2(c) where gold pads have the shining bright color.

Contributed by the Heat Transfer Division for publication in the JOURNAL OF HEAT TRANSFER. Manuscript received by the Heat Transfer Division April 26, 2001; revision received October 18, 2001. Associate Editor: G. P. Peterson.

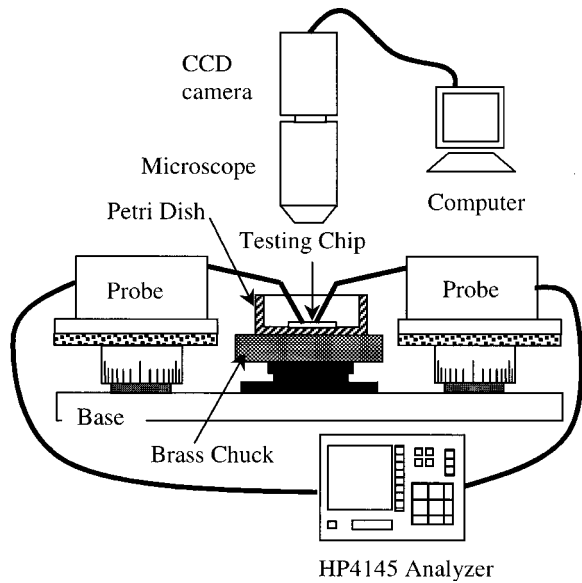


Fig. 1 Schematic drawing of the micro boiling experiment

3 A Lumped Heat Transfer Model

A lumped heat transfer model is developed to investigate the thermal responses of the micro resistor theoretically. This model is graphically shown in Fig. 3 with the following assumptions. First, the polysilicon micro resistor has a uniform temperature along the length of the resistor. This assumption is based on a previous work [17] that line shape polysilicon micro-resistor has relatively uniform temperature distribution away from the boundaries. Since the model is only built on the central portion of the resistor in between the two voltage detecting points, the temperature distribution is assumed to be uniform. Second, the heat loss through the two ends of the micro-resistor are neglected because the cross-section areas of the two ends of the micro-resistor are comparatively much smaller than the areas along the micro resistor. Third, the temperature distribution across the silicon nitride layer underneath the polysilicon resistor is linear. This assumption is based on the fact that the width of the micro-heater is much larger than the thickness of nitride layer. Therefore, the temperature change is approximated as linear within the portion of nitride layer that is underneath the polysilicon resistor. Fourth, the substrate warming

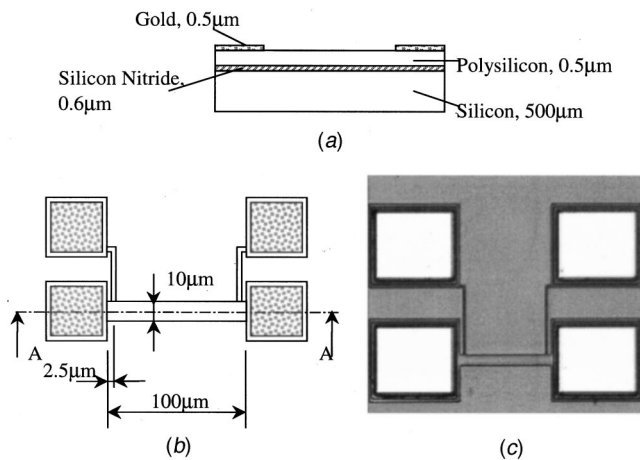


Fig. 2 Schematic diagrams of the polysilicon micro resistor: (a) cross-sectional view; (b) top view; and (c) photograph of a fabricated polysilicon micro resistor.

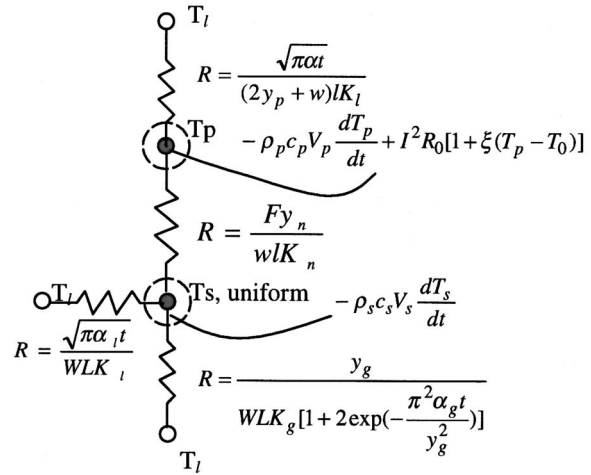
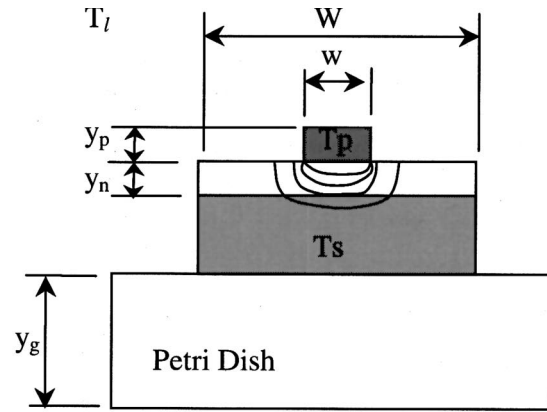


Fig. 3 Schematic drawing of the lumped heat transfer model. The electric analogy is drawn on the right.

effect is an important parameter to be characterized, and the silicon substrate is assumed to have a uniform temperature of T_s to simplify the analysis. However, non-uniform temperature distribution is expected at regions close to the polysilicon micro-resistor. An experimentally determined factor, F , is used to adjust possible errors coming from this assumption. This factor is defined as the extension factor to the thickness of the nitride layer to accommodate the region of non-uniform temperature. Intuitively, this factor will be determined by the thermal conductivity of nitride, silicon, and their geometrical relationships. In this work, this number is experimentally characterized by comparing the analytical prediction with the measured wall temperature. Fifth, heat conduction in liquid is modeled by semi-infinite thermal conduction and both heat convection and radiation are neglected [17]. Sixth, it is assumed that the bottom surface of the Petri dish is at room temperature, since it is in contact with a big brass chuck that is a good heat sink. A lumped, one-dimensional heat transfer model is established graphically as shown in Fig. 3. According to the transient thermal conduction equation, the transient temperature of a slab with temperature fixed at two sides is modeled by [18]

$$T_y = T_1 + (T_2 - T_1) \frac{y}{l} + \frac{2}{\pi} \sum_{n=1}^{\infty} \frac{T_2 \cos n\pi - T_1}{n} \sin \frac{n\pi y}{l} e^{-an^2\pi^2 t/l^2}, \quad (1)$$

Table 1

Parameter	Value	Parameter	Value	Parameter	Value
ρ_p	2320 Kg/m ³	c_p	700 J/KgK	K_n	3.2 W/mK
K_s	141 W/mK	K_l	0.136 W/mK	y_n	0.6 μ m
W	10 μ m	l	95 μ m	y_p	0.5 μ m
R_0	300 Ω	ξ	1.2E-3 /K	α_l	5.9E-8 m ² /s
T_1	294 K	T_0	300 K	ρ_s	2320 Kg/m ³
c_s	700 J/KgK	K_g	1.2 W/mK	y_s	500 μ m
W	1 cm	L	1 cm	y_g	1.8 mm
α_g	5.1E-7 m ² /s	E	6.4E5 J/Kg		

where $T_{1,2}$ are temperatures at two sides of a slab, y is the coordinate along the slab thickness, l is the slab thickness, and α is the thermal diffusivity of the slab. Taking derivative with respect to y and multiplying with material conductivity K , one can obtain the heat flux as

$$K \frac{\partial T_y}{\partial y} = K \left[\frac{(T_2 - T_1)}{l} + \frac{2}{l} \sum_1^{\infty} (T_2 \cos n\pi - T_1) \times \cos \frac{n\pi y}{l} e^{-\alpha n^2 \pi^2 t / l^2} \right] \quad (2)$$

For first-order approximation, only the first term in the summation is considered in the above equation. Based on the above assumptions and energy balance, the heat transfer equations of polysilicon and silicon can be derived as

$$\rho_p c_p \frac{dT_p}{dt} = -\frac{K_n (T_p - T_s)}{y_p F y_n} - \left(\frac{2}{w} + \frac{1}{y_p} \right) K_l \frac{(T_p - T_l)}{\sqrt{\pi \alpha_l t}} + \frac{l^2 R_0 [1 + \xi (T_p - T_0)]}{w l y_p} \quad (3)$$

$$\rho_s c_s \frac{dT_s}{dt} = \frac{w l}{W L} \frac{K_n (T_p - T_s)}{y_s F y_n} - \frac{K_l (T_s - T_l)}{y_s \sqrt{\pi \alpha_l t}} - \frac{K_g T_s - T_l}{y_s y_g} \times \left[1 + 2 * \exp \left(-\frac{\pi^2 \alpha_g t}{y_g^2} \right) \right] \quad (4)$$

The values used in the equations are listed in Table 1. These two equations can be solved simultaneously to obtain the values of T_p (polysilicon micro resistor temperature) and T_s (silicon substrate temperature) with respect to time. The liquid used in the experiments is IPA (Isopropyl Alcohol) [19].

4 Results and Discussion

4.1 General Behavior of Micro-Boiling Phenomenon.

The general behavior of micro-boiling phenomenon is recorded based on the micro-resistor with size of $100 \times 10 \times 0.5 \mu\text{m}^3$ under various constant input currents from 15 to 40 mA. The measured wall temperatures for the first 10 sec are shown in Fig. 4 and the close look of relative temperature changes from Fig. 4 are plotted in Fig. 5. As expected, the measured wall temperature increases as the input current increases. It is found that bubble formation characteristics with respect to input current levels can be classified into three groups. In group I, where the input current is less than 22 mA, no bubble is nucleated and the temperature of the polysilicon micro-resistor remains nearly the same. Group II represents the middle range of input currents between 25 to 30 mA and is the most interesting group in terms of transient bubble formation behavior. The wall temperature increases at the beginning and drops ahead of the bubble formation when a blurry cloud covers the polysilicon micro-resistor as observed through the microscope. The slope of this temperature drop seems to become

steeper as the magnitude of the input current increases and disappears under high input power. For example, this phenomenon is observed when the input current is less than 40 mA for the 10 μm wide resistors and 15 mA for the 5 μm wide resistors. Once a bubble is nucleated, the wall temperature increases and goes above the initial temperature before reaching a steady state. In the final group where the input current is equal or higher than 40 mA, a bubble is formed as soon as the electrical current is applied. There is no detectable temperature drop when the thermal bubble is generated and the resistor temperature continues to increase and the bubble grows before a steady state is reached. In all three groups, it is measured that the temperature of the silicon substrate has also risen and gradually reaches a steady state temperature about 1 to 10°C higher than the room temperature depending on

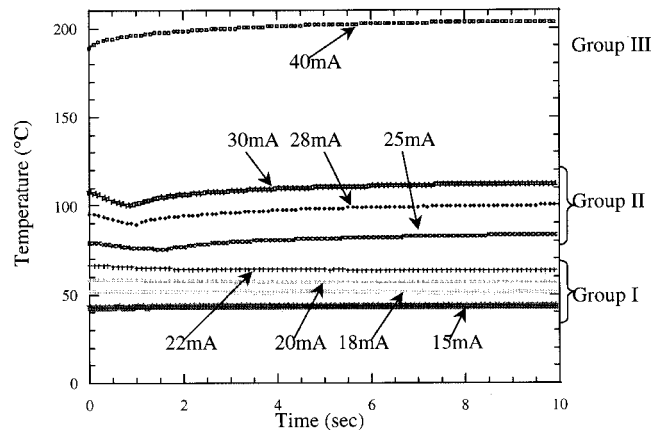


Fig. 4 Measured wall temperature with respect to time on the polysilicon micro resistor of 10 μm wide

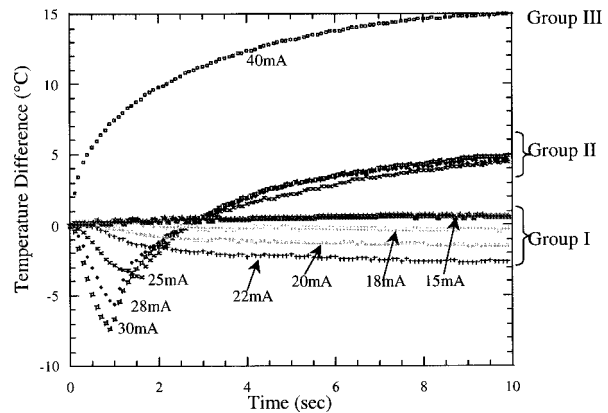


Fig. 5 Relative temperature changes for the transient micro bubble formation on the 10 μm wide polysilicon micro resistor

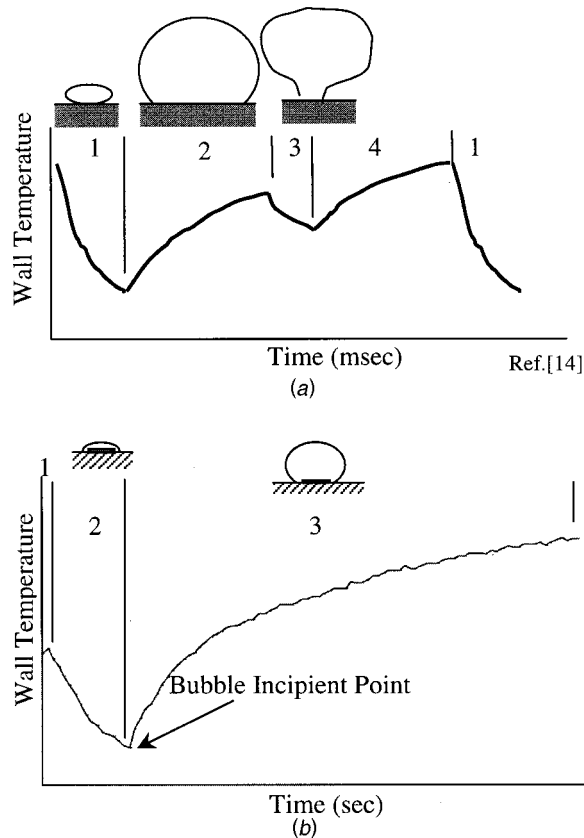


Fig. 6 Comparison of bubble nucleation in macro and micro scales: (a) typical wall temperature history in macro scale boiling experiments; and (b) typical wall temperature history in micro scale boiling on a polysilicon micro resistor.

the level of the input power. It is noted that the dissolved air in bulk liquid may affect the experimental results but is not studied in this work.

4.2 Comparison of Macro and Micro-Boiling Experiments.

Figure 6 illustrates the typical wall temperature of bubble nucleation processes for both macro [20] and micro-scale experiments, respectively. The macro-scale bubble nucleation experiments are generally conducted at pool boiling condition where the liquid is at the saturation state. The micro-scale bubble nucleation test, on the other hand, refers to bubble formation on micro-scale resistive heaters in a pool of cool liquid. For a typical macro-scale boiling process under a constant heating power as shown in Fig. 6(a) [20], formation of bubbles is observed in stage 1. The temperature drop in stage 1 has been explained as the evaporation of a microlayer liquid between the bubble and the heating wall. When the microlayer evaporates and dries out, the boiling process moves to stage 2, where the bubble continues to grow. The wall temperature rises in this stage because of the blockage of the heat flux from the wall to the liquid due to the existence of the bubble. When the bubble grows to a certain size and starts to lift off the wall as shown in stage 3, cool liquid is sucked to the wall to cause a quenching effect. The cool liquid is then heated up gradually in stage 4 to the original temperature, where a new bubble is nucleated and the process repeats itself continuously.

Group II in Fig. 4 and 5 of the bubble nucleation experiments in the micro scale, is discussed and compared with macro scaled boiling experiments due to similarities. One may identify three stages of wall temperature responses on transient bubble formation. In stage 1, the wall temperature jumps right after an electric current is applied and moves up gradually as the substrate temperature rises. The period of this stage is shorter than 0.1 sec for

the 10 μm wide resistor and becomes shorter if the input current level is increased. It is believed that liquid is superheated locally in this stage until naturally generated disturbance induces the evaporation process and moves the micro-boiling process to stage 2. According to the homogeneous bubble nucleation theory [20], there is a nucleus radius under thermodynamic equilibrium. Once the initial bubble nucleus radius is larger than the critical value, the bubble will tend to grow. Otherwise, it will shrink. High current inputs generate high temperature that implies smaller equilibrium nucleus radius. Therefore, the probability that the bubble embryos are larger than the critical size is increased and a large single spherical bubble is induced. This can be the reason causing the temperature profile transits from stage 2 into stage 3. Moreover, high current inputs seem to speed up the evaporation process that causes the wall temperature to drop faster as shown in Fig. 5. As soon as a bubble emerges, the wall temperature increases as shown in stage 3, in which a spherical bubble grows and covers the whole polysilicon micro resistor. The wall temperature increases in this stage because the vapor bubble is blocking the heat dissipation process. The nucleated micro-bubble continues to grow slowly and sticks to the polysilicon micro-resistor due to Marangoni effect [17] and the wall temperature gradually reaches equilibrium.

4.3 Thermal Conduction. According to Eqs. (3) and (4), one can estimate the time constants of the polysilicon micro-resistor and silicon substrate by the following expressions:

$$1/\tau_p \sim \frac{1}{\rho_p c_p y_p} \left(\frac{K_n}{F y_n} - \frac{I^2 R_0 \xi}{w l} \right) \quad (5)$$

$$1/\tau_s \sim \frac{1}{\rho_s c_s y_s} \left(\frac{w l K_n}{W L F y_n} + \frac{K_g}{y_g} \right) \quad (6)$$

where τ_p and τ_s are time constants of polysilicon micro-resistor and silicon substrate, respectively. Substituting values in Table 1 into the above equations, one can find that τ_p is in the order of microseconds, and τ_s is in the order of milliseconds. It implies that in the early stage of the heating process, the temperature of polysilicon micro resistor is not affected by the silicon substrate warming effect and can be estimated by Eq. (3). When the operation period is longer than milliseconds, the substrate warming effect has to be considered.

A modification factor, F , is introduced as a measure of the effective thickness of nitride layer, and this factor accounts modeling errors coming from the simplifications of the model and its magnitude is determined by experiments. Figure 7 shows the measured temperature of the polysilicon micro resistor as well as the predictions from various values of F . It can be observed that when F is equal to 1.47, a good match is achieved. This value is then used in further simulation. Figure 8 shows the simulated temperatures of the 10 μm wide polysilicon micro-resistor and the silicon substrate under an input current of 28 mA. As the result shown in Fig. 8, the polysilicon micro-resistor temperature rises quickly and reaches 95°C in less than 1 millisecond. This result explains the fast temperature responses in Fig. 4 after an input current is applied. Comparatively, it takes a longer time to create a small temperature change on the silicon substrate. In the same figure, the temperature rise for the silicon substrate is not observable until 0.5 second later when the temperature rise of 1°C is predicted. This substrate warming effect explains qualitatively the slow temperature rise on the polysilicon micro resistor before a steady state is reached as shown in Fig. 4 and 5. However, the heat conduction model only predicts the increase but not the drop of temperature with respect to time. Other heat dissipation mechanisms must be considered to characterize the wall temperature drops as observed.

4.4 Thermal Convection. The critical Rayleigh number for the onset of natural convection is calculated to investigate the role of thermal convection in this time dependent micro-boiling experiment

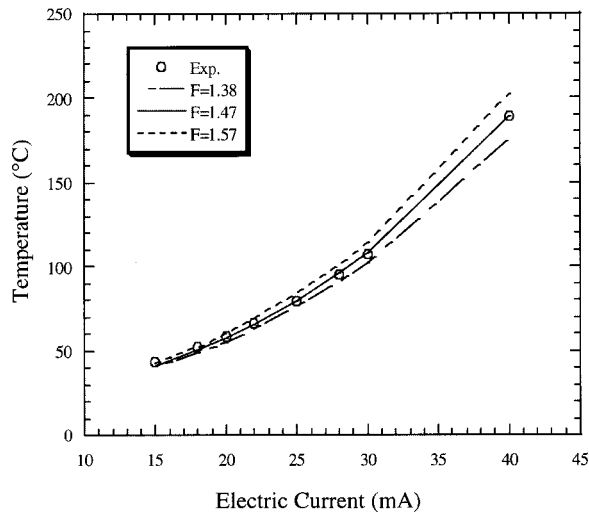


Fig. 7 Simulated initial temperatures of the 10 μm wide micro resistor by using various F values as compared with experimental measurements

$$\text{Ra}_t = \frac{2\pi g \beta q \alpha t^2}{\nu K}, \quad (7)$$

where q is the heat flux to liquid, g is gravity, β is the volume expansion coefficient, ν is dynamic viscosity, and K is thermal conductivity. The model developed in the previous section is used to estimate the heat flux to liquid and other variables. The calculated Rayleigh number is found at least one order of magnitude smaller than the reported critical Rayleigh number [21] when the time period is less than two seconds. Therefore, natural convection is not considered in the mathematical model of Eq. (3) and (4) in the initial stage of bubble formation.

4.5 Evaporation. According to the simulation result presented in Fig. 8, the heating speed in this work is fast in the order of 10^7 K/s. Moreover, a blurry cloud is observed around the micro resistor before the bubble formation. It indicates the film boiling of liquid after the liquid is heated into the metastable state [20] and condensed where the vapor meets with cool liquid. This evaporation of liquid may be considered as the primary reason of temperature drop before a micro bubble is nucleated in the micro

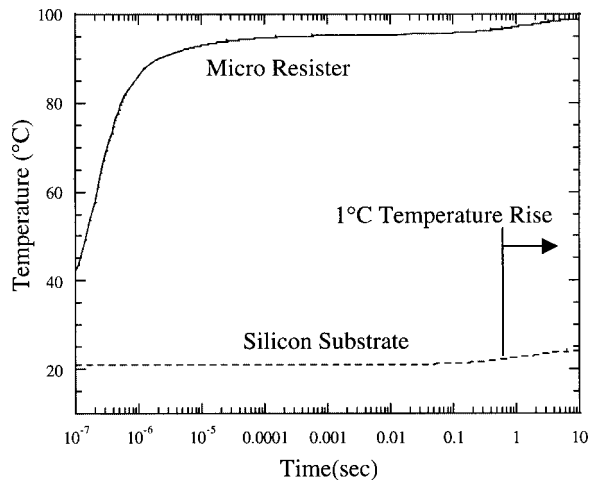


Fig. 8 Simulated results of temperature on polysilicon micro resistor of 10 μm wide and silicon substrate versus time under an input current of 28 mA

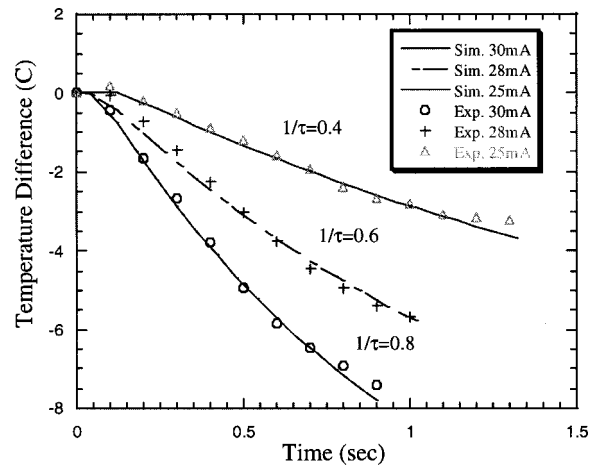


Fig. 9 Comparison of experimental and simulated wall temperatures before the nucleation of a micro-bubble. The equivalent heat transfer coefficient is found to be 10^5 $\text{W}/\text{m}^2\text{C}$

bubble nucleation process. The heat flux of evaporation is modeled as an equivalent heat transfer coefficient and the temperature difference between the polysilicon micro resistor and bulk liquid.

$$h_{\text{evp}}(T_p - T_l) = \frac{\rho_l E}{(w + 2y_p)l} \frac{dV}{dt}, \quad (8)$$

where h_{evp} is the equivalent heat transfer coefficient during the evaporation stage, T_p is the polysilicon micro resistor temperature, T_l is the bulk liquid temperature, E is the latent heat of liquid, and $(w + 2y_p)l$ is the heating area. In order to determine the value of h_{evp} , the model is compared with experimental data from Fig. 5. It is found that the wall temperature drops at a higher rate at the beginning and at a lower rate when approaching the bubble incipient point. Therefore, the equivalent heat transfer coefficient is proposed as

$$h_{\text{evp}} = h_{\text{max}} [1 - e^{-(t - t_{\text{mit}})/\tau}], \quad (9)$$

where t is time, t_{mit} is the time when resistor temperature starts to drop, and τ is an evaporation time constant depending on the level of input power. Therefore, the governing equation of micro resistor of Eq. (3) can be modified in the second stage of bubble formation as

$$\rho_p c_p \frac{dT_p}{dt} = -\frac{K_n}{y_p} \frac{(T_p - T_s)}{F y_n} - \left(\frac{2}{w} + \frac{1}{y_p} \right) h_{\text{evp}} (T_p - T_l) + \frac{I^2 R_0 [1 + \xi(T_p - T_0)]}{w l y_p}. \quad (10)$$

The two parameters in Eq. (9) are found experimentally as shown in Fig. 9 by means of curve fitting. It is found that h_{max} is 7×10^5 $\text{W}/\text{m}^2\text{C}$, and $1/\tau$ is 0.4, 0.6, and 0.8 for input current levels at 25, 28, and 30 mA, respectively. This equivalent heat transfer coefficient is at least two orders of magnitude higher than the natural convection heat transfer coefficient from the macro-scale heat transfer models. Therefore, this result further supports the previous assumption that heat convection only plays a minor role in this stage. The calculated evaporation time constants suggest that higher input current corresponds to smaller time constant and higher evaporation rate. Because the heat flux calculated by the heat evaporation term is much larger than the thermal conduction term, the heat dissipation process in this stage is mainly attributed to liquid evaporation. By substituting these numbers into Eq. (8), where ρ_l is 770 kg/m^3 and E is 640 kJ/kg , the rate of evaporation volume is calculated in the order of 10 nl/sec . In most cases, the

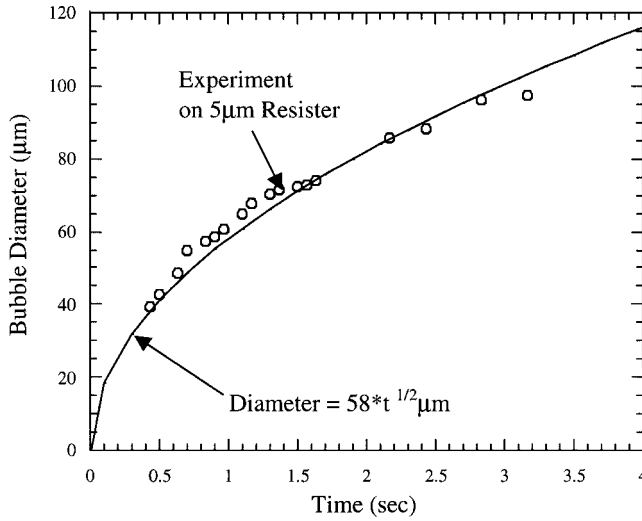


Fig. 10 Bubble size growth rate on a 5 μm micro resistor compared with the heat diffusion controlled bubble growth mode

temperature drop lasts longer than one second and more than 10 nanoliter of liquid has gone through the evaporation-condensation process to cause the observed temperature drop.

4.6 Bubble Growth Rate. It is observed that the bubble formation in Group II of Fig. 4 is randomly scattered along the temperature drop curve in stage 2 of the micro bubble formation process. The possible reason of the transition into a spherical bubble may be the instability of vapor-liquid interface that is agitated by local fluctuation in combination with the readiness of enough metastable state of liquid that can overcome the cool liquid to form a spherical bubble. When a bubble is formed, the wall temperature rises in a manner similar to the second stage in the macro-scaled boiling process. It is believed that the heat dissipation path from the polysilicon micro resistor surface to liquid is partially blocked by the vapor bubble on top. Therefore, temperature rises with the increase of bubble size to reach a new equilibrium temperature.

As described in a previous report [20], thermal bubble growth can mainly be classified into two modes in macro-scale bubble nucleation experiments. The first mode occurs at the initial stage of bubble growth that is hydrodynamically controlled and dominated by liquid inertia and the bubble size increases proportionally to time, $D \propto t$. The second mode occurs at the later stage of bubble growth that is heat diffusion controlled. The bubble grows at a slower rate than in the hydrodynamically controlled mode and is proportional to the square root of time, $D \propto t^{1/2}$. The experimental data on a 5 μm wide micro-resistor is extracted by moving the start point of time to the time when a bubble is nucleated. The bubble diameter is measured from the captured images taken on top of the micro-resistor by the CCD camera, and graphed along with time by circular markers as shown in Fig. 10. It is found that the bubble diameter, D , can be represented as $D = 2Ct^{1/2}$, where C is a constant and t is time. The close match between the markers and the curve indicates that the bubble growth rate on the micro resistor at this stage is dominated by heat diffusion as $D \propto t^{1/2}$.

This relation between bubble size and time is further applied to extend the mathematical model to the bubble growth stage. Two assumptions are made and graphically presented in Fig. 11. First, the bubble is spherical with a uniform temperature at the saturation point. Although the temperature at the bottom portion of the bubble is expected to be higher than the top portion, this assumption is made to simplify the analysis. Second, it is assumed that the bottom of the bubble is in contact with the substrate as shown in Fig. 11 due to a strong local Marangoni effect and the contact

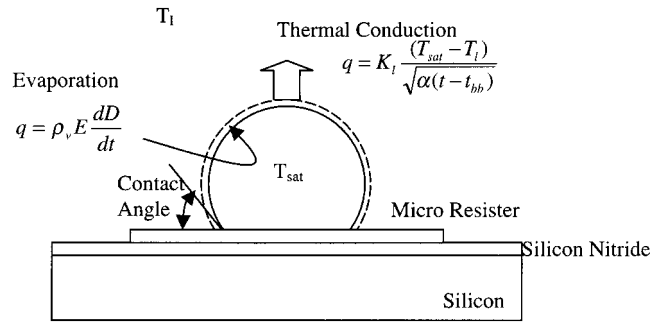


Fig. 11 Schematic drawing of the heat transfer mechanism in bubble growth model

angle is adopted from a previous report [22] as 30 deg. Third, it is further assumed that the bottom of the bubble is in thermal equilibrium with the substrate (no heat transfer) to simplify the problem. In reality, a thin liquid film and thermal gradient with magnitudes may exist depending on the temperature profile of the substrate surrounding the micro heater and a three-dimensional analysis is necessary to model this effect. Fourth, the heat conduction between the bubble/liquid interfaces is assumed as a constant heat source to an infinite field because the bubble temperature is assumed staying at the saturation point. By the above assumptions and energy balance of micro-resistor with heat generation of Joule heating, heat dissipation of the substrate, liquid, and bubble growth, Eq. (1) can be modified as

$$\rho_p c_p \frac{dT_p}{dt} = - \frac{K_n (T_p - T_s)}{y_p F y_n} - \frac{A_{\text{evp}} h_{\text{evp}} (T_p - T_l) + A_{\text{bb}} h_{\text{bb}} (T_p - T_{\text{sat}})}{w l y_p} + \frac{l^2 R_0 [1 + \xi (T_p - T_0)]}{w l y_p} \quad (11)$$

$$A_{\text{evp}} = l(w + 2y_p) - A_{\text{bb}}; \quad A_{\text{bb}} = D(w + 2y_p) \sin \theta$$

$$h_{\text{evp}} = h_{\text{max}} [1 - e^{-(t - t_{\text{init}}/\tau)}],$$

where A_{evp} and A_{bb} are areas of the micro resistor that are not covered by the bubble, h_{evp} is the equivalent heat transfer coefficient of evaporation experimentally determined previously, h_{bb} is the equivalent heat transfer coefficient of the bubble, T_{sat} is the saturation temperature of the liquid, D is the diameter of the bubble, and θ is the contact angle of the bubble with the heater that is approximated as 30 deg from the picture in a previous work [22]. The variation of this angle can affect the magnitude of the bubble growth rate and this number is used for a first-order approximation. The equivalent heat transfer coefficient of the bubble is derived from the energy balance of the heat transferred into the bubble from the micro resistor with the heat dissipation out of the bubble by evaporation and heat conduction to the liquid as illustrated in Fig. 11:

$$A_{\text{bb}} h_{\text{bb}} (T_p - T_{\text{sat}}) = \left[\rho_v E \frac{dD}{dt} + K_l \frac{(T_{\text{sat}} - T_l)}{\sqrt{\alpha(t - t_{\text{bb}})}} \right] A_{\text{sph}} \quad (12)$$

$$A_{\text{sph}} = \frac{\pi D^2 (1 + \cos \theta)}{2},$$

where ρ_v is the vapor density, E is the latent heat of the liquid, t_{bb} is the time when the bubble is formed, and A_{sph} is the interface area of the bubble and the liquid. In this stage, the evaporation and condensation processes are competing with each other. If the diameter of the bubble increases with time, extra energy is supplied to the bubble for the extra evaporation. Otherwise, the bubble

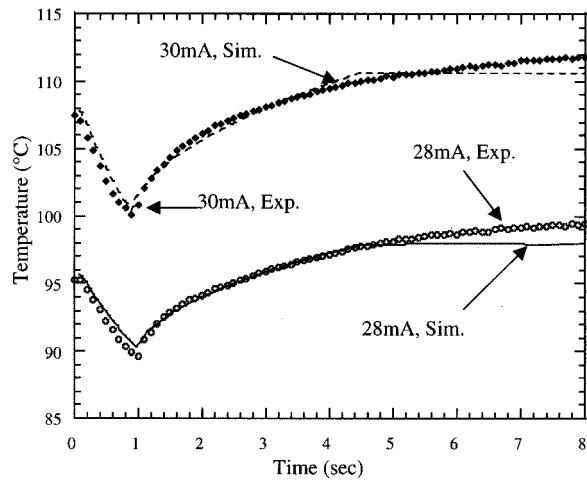


Fig. 12 Comparison between experimental data and simulation on a 10 μm wide of micro-resistor under constant electrical current input. The constant of the bubble size growth rate is 50 $\mu\text{m}/\text{sec}^{1/2}$ in each current level.

shrinks due to extra condensation. By substituting the areas A_{bb} and A_{sph} into Eq. (12), the equivalent heat transfer coefficient is derived as

$$h_{bb} = \left[\rho_v E \frac{dD}{dt} + K_l \frac{(T_{sat} - T_l)}{\sqrt{\alpha(t - t_{bb})}} \right] \frac{\pi D(1 + \cos \theta)}{2(w + 2y_p) \sin \theta (T_p - T_{sat})} \quad (13)$$

According to the result obtained from Fig. 10, the bubble size growth rate is modeled by the thermal diffusion controlled bubble growth mode as

$$\frac{dD}{dt} = \frac{C}{\sqrt{t - t_{bb}}}, \quad (14)$$

where C is the bubble growth rate constant and is determined by curve fitting with the experimental results as 29 and 50 $\mu\text{m}/\text{sec}^{1/2}$ for 5 μm and 10 μm wide resistors, respectively. Combining Eqs. (2), (11), (13), and (14), a first-order approximation model is developed for this bubble growth stage.

Figure 12 shows the simulation results based on the models of Eq. (10) and Eq. (11) and experimental data. It is found that the models match the experimental data well until the time reaches 5 sec when the models underestimate the experimental temperature. The deviation of the simulated temperature from the experimental data may be resulted from the decrease of the bubble growth rate, the simplifications of the model in various aspects such as the contact angle, and the warming effect of the petri dish. For example, the bubble growth rate decreases more than the mode prediction as shown in the later stage in Fig. 10 in reality. It causes the over prediction of the cooling effect in the model such that the simulated temperature is lower than the experimental data.

5 Conclusion

This paper investigates transient bubble formation on micro strip resistors under various levels of constant electrical current input. The transient temperature variations are classified into three groups by the level of input currents. When the constant input current is lower than 25 mA, the wall temperature stays nearly constant and no bubble is nucleated. For the constant input current between 25 to 30 mA, the wall temperature increases initially, quickly drops afterwards until a bubble is formed, and then increases until reaching steady state. For the third group of high input current, the wall temperature rises sharply as soon as the current is applied and a bubble is formed. Among the three

groups, Group II has very interesting transition phenomena that are classified into three stages with respect to time and are investigated extensively in this paper. Mathematical models are established to estimate the resistor temperature during the micro boiling process. It is found that this heat conduction based model is capable of predicting the resistor temperature in the first stage of the boiling heat transfer. The time constant for the resistor temperature is calculated in the microsecond range and in the millisecond range for the silicon substrate. The evaporation of liquid is identified as the key mechanism that causes the resistor temperature to drop before the bubble nucleation in the second stage. Based on the experimental measurements and a simplified, first-order model, an equivalent heat transfer coefficient for the second stage is found to be in order of $7 \times 10^5 \text{ W}/\text{m}^2\text{°C}$, and the evaporation time constants are found as, 2.5, 1.67, and 1.25 sec for the input current levels of 25, 28, and 30 mA, respectively on a 10 μm wide micro-resistor. The incipient point of micro-bubble formation is found randomly distributed during this wall temperature drop period with a trend of earlier occurrence in higher input current. This is probably due to the instability of vapor-liquid interface in the stage of strong evaporation process. Higher electrical current will generate bubbles in shorter time at a higher temperature. After a spherical bubble is found, the bubble growth rate is found proportional to the square root of time on both 5 μm and 10 μm wide of micro resistors. The bubble diameter growth rate constant C is found as 29 $\mu\text{m}/\text{sec}^{1/2}$ in the case of 5 μm wide micro-resistor, and 50 $\mu\text{m}/\text{sec}^{1/2}$ in the case of 10 μm wide micro-resistor.

Acknowledgment

The authors would like to thank Dr. Chuan-Hsien Ku for discussion and assistance on experimental equipments. The work is supported in part by an NSF CAREER award (ECS-0096098) and a DARPA/MTO/MEMS grant (F30602-98-2-0227).

Nomenclature

C	= bubble diameter growth rate constant
c	= specific heat
D	= diameter of spherical bubble
E	= latent heat
F	= modification factor
g	= gravity
h	= heat transfer coefficient
K	= thermal conductivity
l	= length q heat flux
R	= electrical resistance
T	= temperature
t	= time
w	= width
y	= thickness

Greek Symbols

ρ	= density
ξ	= thermal coefficient of resistance
α	= thermal diffusivity
β	= thermal expansion coefficient
ν	= dynamic viscosity
τ	= time constant

Subscripts

0	= reference temperature at 300 K
bb	= bubble
evp	= evaporation
g	= Petri dish
i	= interface
l	= liquid
n	= silicon nitride
p	= polysilicon
s	= silicon
sat	= saturation

References

- [1] Cotter, T. P., 1984, "Principles and Prospects of Micro heat Pipes," *Proc. 5th Int'l. Heat Pipe Conf.*, Tsukuba, Japan, pp. 328–335.
- [2] Bar-Cohen, A., 1983, "Thermal Design of Immersion Cooling Modules for Electronic Components," *Heat Transfer Eng.*, **4**, No. 3-4, pp. 35–50.
- [3] Nielsen, N. J., 1985, "History of Thinkjet Printerhead Development," *HP Journal*, **36**, No. 5, pp. 4–10.
- [4] Lin, L. and Pisano, A. P., 1994, "Thermal Bubble Powered Microactuators," *Microsystem Technol.*, **1**, pp. 51–58.
- [5] Lin, L. and Pisano, A. P., 1998, "Thermal Bubble Formation on Polysilicon Micro Resistors," *ASME Journal of Heat Transfer*, **120**, No. 3, pp. 735–742.
- [6] Yuan, H., Oguz, H. N., Prosperetti, A., 1999, "Growth and Collapse of a Vapor Bubble in a Small Tube," *Int. J. Heat Mass Transf.*, **42**, pp. 3643–3657.
- [7] Tsai, J. H., and Lin, L., 2001, "A Thermal Bubble Actuated Micro Nozzle-Diffuser Pump," *IEEE 2001 Micro Electro Mechanical System Workshop*, Interlaken, Switzerland, pp. 409–412.
- [8] Evans, J. D., and Liepmann, D., 1999, "The Bubble Spring and Channel (BSAC) Valve: An Actuated, Bi-stable Mechanical Valve for In-Plane Fluid Control," *Transducer '99*, Sendai, Japan, pp. 1122–1125.
- [9] Lin, L., Udell, K. S., and Pisano, A. P., 1994, "Liquid-Vapor Phase Transition and Bubble Formation in Micro Structures," *Therm. Sci. Eng.*, **2** pp. 52–59.
- [10] Yang, W. J., and Tsutsui, K., 2000, "Overview of Boiling on Microstructures-Macro Bubbles From Micro Heaters," *Microscale Thermophys. Eng.*, **4**, No. 1, pp. 7–24.
- [11] Cole, R. 1974, "Boiling Nucleation," in *Advances in Heat Transfer*, Vol. 10, Academic, New York.
- [12] Hsu, Y. Y., 1962, "On the size Range of Active Nucleation Cavities on a Heating Surface," *ASME Journal of Heat Transfer*, **84C**, pp. 207–216.
- [13] Sernas, V. and Hooper, F. C., 1969, "The Initial Vapor Bubble Growth on a Heated Wall during Nucleation Boiling," *Int. J. Heat Mass Transf.*, **12**, pp. 1627–1639.
- [14] Moore, F. D. and Mesler, R. B., 1961, "The Measurement of Rapid Surface Temperature Fluctuations During Nucleate Boiling of Water," *AIChE J.*, **7**, No. 4, pp. 620–624.
- [15] Koester, D., Mhedevan, R., and Marcus, K., 1999, *Multi-User MEMS Processes (MUMPS) Design Handbook*, rev. 4, May 1999, Cronos Integrated Microsystems, 3021 Cornwallis Road, Research Triangle Park, NC, 27709.
- [16] Mastrangelo, C. H., 1991, Ph.D. thesis, University of California at Berkeley, Berkeley, CA.
- [17] Lin, L., 1993, Ph.D. thesis, University of California at Berkeley, Berkeley, CA.
- [18] Carslaw, H. S., and Jaeger, J. C., 1959, *Conduction of Heat in Solids*, 2nd ed., Oxford University Press, London, pp. 99–100.
- [19] Vargaftik, N. B., 1975, *Tables on the Thermophysical Properties of Liquids and Gases*, Hemisphere Pub. Corp., Bristol, PA, pp. 418–420.
- [20] Stralen, S. V., and Cole, R., 1979, *Boiling Phenomena*, Vol. 1, Hemisphere Pub. Corp., Bristol, PA, pp. 454–456.
- [21] Goldstein, R. J., Volino, R. J., 1995, "Onset and Development of Natural Convection Above a Suddenly Heated Horizontal Surface," *ASME Journal of Heat Transfer*, **117**, No. 4, pp. 808–821.
- [22] Shimokubo, T., Takagi, S., and Inoue, T., 1998, "Boiling Bubble Behavior from the Micro Heater," *Proc. 35th Heat Transfer Symp. of Japan*, pp. 173–174.